Local spin-coupled distortions in multiferroic hexagonal HoMnO$_3$

T. A. Tyson,[1,2] T. Wu,[1] K. H. Ahn,[1,2] S.-B. Kim,[2] and S.-W. Cheong[2]

[1]*Department of Physics, New Jersey Institute of Technology, Newark, New Jersey 07102, USA*

[2]*Department of Physics and Astronomy and Rutgers Center for Emergent Materials,*
Rutgers University, Piscataway, New Jersey 08854, USA

Local structural measurements have been performed on hexagonal HoMnO$_3$ in order to ascertain the specific changes in bond distances, which accompany magnetic ordering transitions. The transition from the paramagnetic to the antiferromagnetic (noncollinear) phase near $\sim$70 K is dominated by changes in the *a-b* plane Mn-Mn bond distances. The spin rotation transition near $\sim$40 K involves both Mn-Mn and nearest-neighbor Ho-Mn interactions while the low-temperature transition below 10 K involves all interactions, Mn-Mn, Ho-Mn (nearest and next nearest), and Ho-Ho correlations. These changes in bond distances reveal strong spin-lattice coupling. The similarity in magnitude of the change in J(Mn-Mn) and J(Ho-Mn) enhances the system frustration. The structural changes are interpreted in terms of a model of competing spin order and local structural distortions. Density-functional calculations are used to estimate the energies associated with ionic displacements. The calculations also reveal asymmetric polarization of the charge density of Ho, O3, and O4 sites along the *c* axis in the ferroelectric phase. This polarization facilitates coupling between Ho atoms on neighboring planes normal to the *c* axis.

PACS number(s): 77.80.B−, 78.70.Dm

I. INTRODUCTION

The existence and coupling of distinctly different types of long-range order is stimulating much interest from a fundamental science perspective. The rare earth hexagonal manganites corresponding to systems with the chemical formula REMnO$_3$ [rare-earth (RE) ions with small radii such as Sc, Y, Ho, Er, Tm, Yb, and Lu] exhibit both ferroelectric and magnetic order. In this specific class of materials the transition to the ordered ferroelectric state (T_{FE}) occurs between $\sim$800 and $\sim$1200 K while the ordered magnetic states occur at significantly lower temperature ($T_N \sim 80$ K). This hexagonal structure can also be stabilized in large radius cation systems by quenching them from high temperature or by depositions on substrates which induce strain.[1–7]

In the hexagonal structure, the Mn^{3+} ions form a triangular planar lattice where the Mn spins are coupled indirectly through the planar oxygen atoms. Locally the Mn ions are incorporated into MnO$_5$ polyhedra (bipyramids) with three oxygen atoms surrounding the Mn atom in a plane and two apical oxygen atoms above and below the plane completing the polyhedron. Excluding the oxygen atoms, the Mn ions form a triangular two-dimensional lattice, with each two dimensional layer separated by RE site ions.

The degree of frustration in these systems, indicated by the ratio of the Curie-Weise constant (derived from $1/\chi$) to the Néel temperature, approaches 10 in the hexagonal systems.[4] The frustration is relieved by transition into a unique in-plane (*a-b* plane) magnetic ordering, in which the Mn ion moments are pointed 120° relative to each other. In the systems with open 4*f* shells (REMnO$_3$), a series of magnetically ordered states are found since, it is believed, that the spins on the RE ions can both couple with the Mn ions and each other and order magnetically and at low temperatures.[6,7] In HoMnO$_3$, for example, neutron diffraction measurements reveal a 90° in-plane rotation of the Mn

spins near $\sim$40 K (T_{SR}) followed by magnetic ordering of the Ho sites below $\sim$5 K (T_{Ho}).

Anomalies in the dielectric constants, the linear expansion coefficients and phonon frequencies suggest a coupling between the magnetic and ferroelectric order at low temperature.[8,9] In HoMnO$_3$, sharp features are observed at T_{SR} and T_{Ho}. Heat capacity and magnetic susceptibility measurements in magnetic field reveal that while the position of T_N is stable with respect to external magnetic fields the T_{SR} transition temperate is strongly field dependent and moves to lower temperature with increasing magnetic fields.[5] Moreover, a complex multiphase structure is found at low temperature. In magnetization studies on HoMnO$_3$ no slope changes are found at T_N. However, changes in slope were found at T_{SR} and T_{Ho}. The abrupt changes in the *c*-axis magnetization at T_{SR} were attributed to changes in the magnetic order of the Ho^{3+} ions since the Mn spin is confined to the *a-b* plane. A lambda-type anomaly occurs in the heat capacities at T_N in zero magnetic field. The peaks at T_{SR} and T_{Ho} are found to exhibit sharp onsets suggesting first-order transitions. A complex phase diagram is revealed in the *H-T* plane at low temperature.

Under pressure, the sharp peak in the dielectric constant seen at T_{SR} moves to lower temperature and is reduced in amplitude as pressure is increased from 0.1 to 1.7 GPa.[8] In addition, the *a-b* plane lattice parameter is more readily compressed with pressure than the *c*-axis lattice parameter.[10] Hence, the in plane Mn-Mn correlation may be preferentially modified by pressure. This suggests that strain may suppress the magnetic transitions in HoMnO$_3$ and other hexagonal REMnO$_3$ systems. Indeed, as a result of tensile strain, the magnetic structure of *c*-axis oriented epitaxial HoMnO$_3$ films differs from that of bulk system and has a significantly reduced T_N ($\sim$20 K lower).[11,12]

In the low-temperature ferroelectric phase, it is argued that there is a tilting of the MnO$_5$ polyhedra toward O(3) at the threefold rotation center and a buckling of the RE

plane.[13] RE is off the center of two in-plane (*a-b* plane) oxygen atoms along the *c*-axis and this produces a dipole along the *c*-axis in one O-RE-O-RE chain along the *c* axis. The number of RE(1) chains and RE(2) chains are not equal and, hence, a net dipole along *c* is produced. The low-temperature moment on the Mn site is found to vary between $\sim 3\mu_B$ and $\sim 3.5\mu_B$ (not $4\mu_B$ expected for a Mn^{3+} ion) possibly due to the persistence of strong fluctuations even below the ordering temperature of the RE site. In $LuMnO_3$, strong magnetic diffuse scattering exist up to approximately $3T_N$ indicating that spin fluctuation exist up to this temperature. Doping with Zr stabilizes the diffuse scattering down to very low temperatures suggesting short range antiferromagnetic clusters.

Recent work suggest that there is no rehybridization or change in the chemical bonding between the high-temperature paraelectric and low-temperature ferroelectric phases in $YMnO_3$.[2] The Born effective charges are found to be close to the values expected based on the formal valence values with respect to the high-temperature unit cell. A large in-plane (*a-b* plane) oxygen (Op) displacement was shown to be composed of two components by group theoretical analysis. K_3 corresponds to a tilting of the Mn-O polyhedra leading to a tripling of the unit cell volume and a Γ-point component related to Y-Op displacements and noncancelling polarization due to the buckling of the MnO_5 pyramids. Further analysis of the combined group theoretical and density functional analysis of $YMnO_3$ revealed a single mode (K_3) at the boundary couples to the polarization.[14] The structural changes resulting from softening of the K_3 mode induces a net polarization. The K_3 mode involves motion of Y at the $2a$ and $4b$ positions position (Y1 and Y2) and oxygen at the $6c$, $2a$, and $4b$ positions (O1, O2, O3, and O4). The dominant displacements are for the Y1 and O3 ions along the *c* axis.

Neutron diffraction measurements reveal the long range order of the Ho moments onsets at T_{SR} and that the ordered moment on the Mn site is enhanced below the T_{Ho}. This shows that the Mn and Ho spin sublattices are coupled. Measurement of the spin wave dispersion for the spins on the Mn^{3+} gives good agreement with a two dimensional nearest neighbor Heisenberg model.[3]

In this work, detailed temperature-dependent local structural measurements were conducted on hexagonal $HoMnO_3$ in order to determine, which bond pairs were associated with the changes in the dielectric constants at the magnetic ordering temperatures. The local structural measurements enable a microscopic level assessment of the spin-lattice coupling on the level of specific pairs of atoms. (The x-ray absorption measurements at the Ho-*L3* and Mn *K*-edges probe bond pairs and as compared to scattering measurements which yield unit cell averaged atomic positions. This approach enables a direct examination of the atoms pairs which couple magnetically.) The transition from paramagnetic to the anti-ferromagnetic (noncollinear) phase near ~ 70 K (T_N) is dominated by changes in the *a-b* plane Mn-Mn bond distances. The spin-rotation transition (T_{SR}) near ~ 40 K involves both Mn-Mn and nearest-neighbor Ho-Mn interactions while the low-temperature transition (T_{Ho}) below 10 K involves all interactions, Mn-Mn, Ho-Mn (nearest and next nearest), and Ho-Ho correlations. Density-functional calcula-

tions reveal asymmetric polarization of the charge density of Ho, O3 and O4 sites along the *c* axis in the ferroelectric phase.

II. EXPERIMENTAL AND COMPUTATIONAL METHODS

Polycrystalline samples of hexagonal $HoMnO_3$ were prepared by solid state reaction. X-ray absorption samples were prepared by grinding and sieving the material (500 mesh) and brushing it onto Kapton tape. Layers of tape were stacked to produce a uniform sample for transmission measurements with jump $\mu t \sim 1$. Spectra were measured at the National Synchroton Light Source beamline X23B at Brookhaven National Laboratory. Measurements were made on warming from 6 to 300 K in a sample attached to the cold finger of a cryostat. Two to six scans were taken at each temperature. The uncertainty in temperature is <0.2 K. At the Mn *K* edge, a Mn foil reference was employed for energy calibration. The reduction of the x-ray absorption fine-structure (XAFS) data was performed using standard procedures.[15]

To treat the atomic distribution functions on equal footing at all temperatures the spectra were modeled in *R* space by optimizing the integral of the product of the radial distribution functions and theoretical spectra with respect to the measured spectra. Specifically the experimental spectrum is modeled by $\chi(k)=\int \chi_{th}(k,r)4\pi r^2 g(r)dr$, where χ_{th} is the theoretical spectrum and $g(r)$ is the real space radial distribution function based on a sum of Gaussian functions [$\chi(k)$ is measured spectrum][16] at each temperature as in Ref. 17. Theoretical spectra for atomic shells[18] were derived from the room temperature crystal structure[7] shown in Fig. 1. For the Mn *K* edge, the *k* range $2.54 < k < 11.5$ $Å^{-1}$ and the *R* range $0.67 < R < 4.08$ Å were used while for the Ho *L3* edge the *k* range $2.96 < k < 14.15$ $Å^{-1}$ and *r* range $1.27 < R < 4.08$ Å were utilized. Coordination numbers for the atomic shells were fixed to the crystallographic values. For the Mn *K* edge and the Ho *L3* edges S_0^2 (accounting for electron loss to multiple electron excitation channels) values were fixed at 0.80 and 0.96, respectively. The Gaussian widths and positions were fit for each component. Representative XAFS data and fits at 170 K are shown in Figs. 2 and 3 for the Mn *K* edge and Ho *L3* edge, respectively. The limited energy range at the Mn *K* edge constrained our modeling to the shells: $\langle$Mn-O1,Mn-O2,Mn-O3$\rangle$, Mn-O4, Mn-Mn, and Mn-Ho (long, short). For the Ho *L3* edge, modeling was restricted to the $\langle$Ho-O$\rangle$, Ho-Mn(short), Ho-Ho, and Ho-Mn(long) distances (see Fig. 1 for structural model).

To estimate the force constants local spin density approximation (LSDA) based functional calculations in the projector augment wave approach[19] were carried out. Full optimization was conducted for both lattice parameters and atomic positions and the LSDA+*U* approximation was implemented to obtain the relaxed structure. The ground-state structure was optimized so that forces on each atom were below 7×10^{-5} eV/Å. Self-forces along the *x*, *y*, and *z* directions were computed for all atoms based on 0.03 Å displacements. The force constants were derived from combined positive and negative displacements.
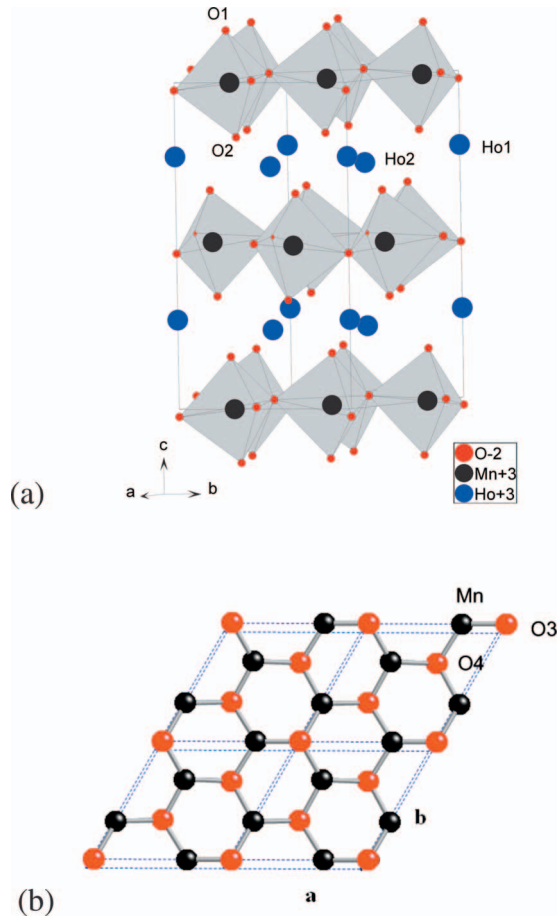
FIG. 1. (Color) The crystal structure of hexagonal HoMnO₃ showing the MnO₅ bipyramids in (a) and the triangular lattice of Mn ions linked by oxygen atoms in (b).

To understand the charge distribution and bonding between the atoms in unit cell, calculation of the charge density within the local spin density approximation ($U/J=0$) was carried out using the all-electron full potential linear augmented plane-wave plus local orbital (FPLAPW+lo) method implemented in the WIEN2K code.[20] The derived charge density plots were found to be qualitatively insensitive to the use of finite U/J parameters.
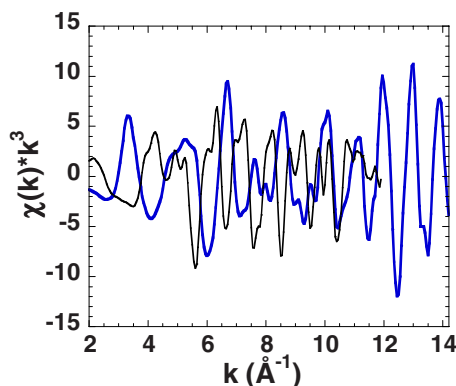

FIG. 2. (Color online) XAFS data at 170 K for the Mn K edge (thin line) and Ho $L3$ edge (thick line).
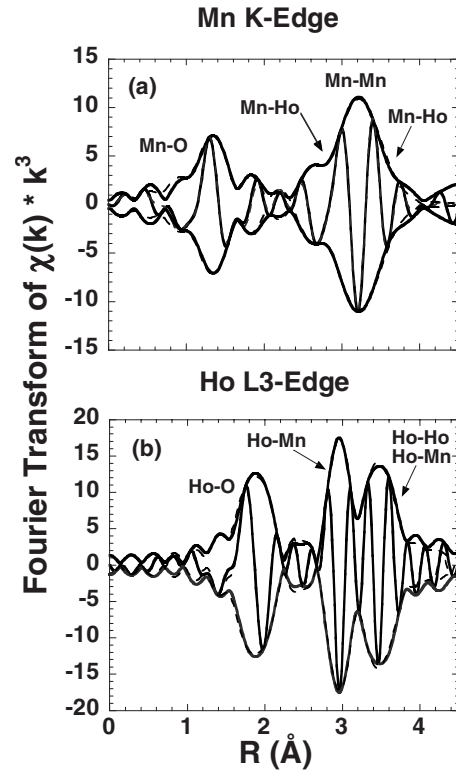

FIG. 3. Fourier transform of the XAFS data taken at 170 K (radial structure functions) for structure about the (a) Mn and (b) Ho sites. The thin dashed thin lines are fits to the data. Peaks are shifted to lower R values from real distances by atomic phase shifts.

III. RESULTS AND DISCUSSION

In Fig. 1(a) we show the structure of HoMnO₃ in the room temperature ferroelectric phase. Note that the Mn ions lie in a plane [Fig. 1(b)] forming a triangular lattice and are linked through O3 and O4 oxygen sites. Normal to this plane, the Mn ions are bonded to O1 and O2 apical oxygen atoms. We refer to the interactions between in-plane Mn ions (via the oxygen ions) as $J1$ exchange with an average Mn-Mn distance of ~3.5 Å and average Mn-O-Mn bond angle of ~119°. (Strictly speaking there is not perfect triangular symmetry and hence there are multiple $J1$ interactions. However, we are just attempting to rank the sizes of the various types of interactions.) The Ho1 and Ho2 ions form a triangular plane, which is buckled in the low temperature structure. The Ho sites interact with each other through the O1 and O2 apical oxygen sites below or above the buckled Ho plane. The average nearest neighbor Ho-Ho distance is ~3.6 Å with average Ho-O-Ho angles of ~102°. In addition to the Ho-Ho interactions and the Mn-Mn interactions there are also interactions between the Mn and Ho ions through the O1 and O2 apical oxygen ions. As a result of the bucking of the Ho planes the Ho-Mn bonds occur at two distinct distances which we call Ho-Mn$_{short}$ and Ho-Mn$_{long}$ with bond distances of ~3.3 and ~3.7 Å, respectively. The corresponding Mn-O-Ho bond angles are 106° and 125°, respectively. We label the long and short interactions as $J3L$ and $J3S$. Even though the magnetic structure obtains a unique spin configurations at low temperature for the two-
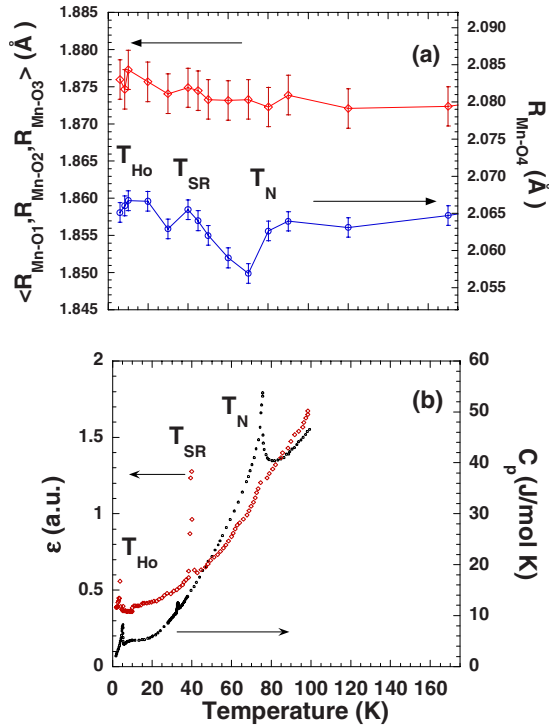
FIG. 4. (Color online) Mn-O bond distances as a function of temperature. The predominantly out-of-plane average of the Mn-O1, Mn-O2, and Mn-O3 bonds is shown as the upper curve and the in-plane Mn-O4 bond in shown as the lower curve [both in panel (a)]. For comparison, the heat capacity (from Ref. 5) and the dielectric constant (from Ref. 8) as a function of temperature are shown in panel (b).
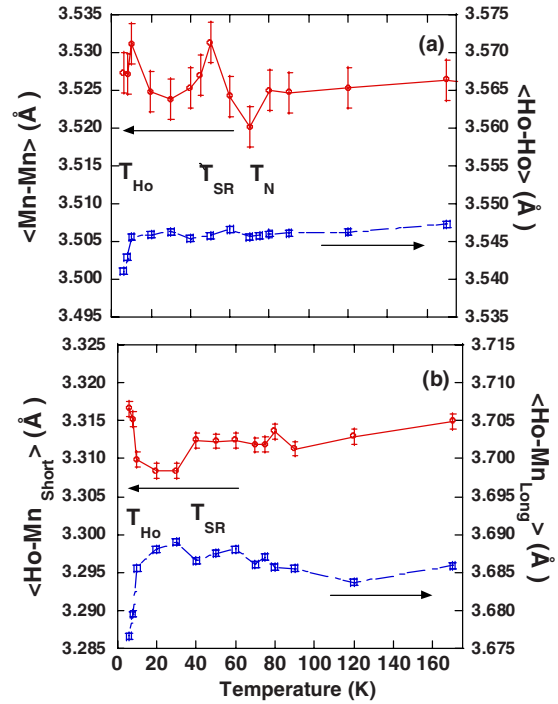

FIG. 5. (Color online) The average Mn-Mn bond distance and average Ho-Ho bond distance are shown as the upper and lower curves in panel (a), respectively. In panel (b) the average Ho-Mn bond distances (short and long) are shown. The long bond exhibits a drop at the Ho ordering temperature while a dip and rise are observed in the short Ho-Mn distance at the Mn reordering temperature and the Ho ordering temperatures.

dimensional Mn triangular lattice, the presence of the Ho ions with localized $4f$ orbitals will impact the magnetic structure at low temperature. The $J1$ and $J3S$ interactions should dominate at higher temperature due to the larger angles and/or shorter distances between the metal sites. This should be followed by the $J3L$ and the $J2$ interactions [where the $J2$ interaction corresponds to in-plane Ho-Ho correlations (see Fig. 7 for all interactions)]. We now look at the temperature dependence of the local structure to identify the specific bond changes associated with magnetic ordering temperatures.

X-ray absorption measurements at the Mn K edge and Ho $L3$ edge enable us to examine the local structure about the Mn and Ho ions, respectively (Figs. 2 and 3). Temperature dependent structural analysis yield evidence for structural changes at magnetic ordering temperatures. In Fig. 4(a) we show the temperature dependence of the average Mn-O1, Mn-O2, and Mn-O3 bond distances ($\langle R_{Mn-O1}, R_{Mn-O2}, R_{Mn-O3} \rangle$) giving mainly the out-of-plane bond distance. At the level of the measurements no changes in out-of-plane Mn-O bond distances are seen. However, we note that the changes in the Mn-O3 bond are expected to anticorrelate with those of the Mn-O4 bond (as indicated by diffraction experiments).[4] The in-plane Mn-O4 bond distance, on the other hand, displays anomalies at all magnetic transitions T_N, T_{SR}, and T_{Ho}, the largest change occurring at T_N. For comparison we show in Fig. 4(b) the changes in the

heat capacity (from Ref. 5) at these temperatures revealing that they correspond to magnetic ordering transitions. Moreover, the anomalies in the dielectric constants (from Ref. 8) at the magnetic ordering temperatures support the argument for strong spin-lattice coupling. Earlier measurements of the dielectric constants on single crystals of $YMnO_3$ and $LuMnO3$ show anomalies at T_N for electric fields in the *ab*-plane but none for the electric fields along the *c* axis.[8] It is argued that the interaction are dominated by interactions within the *ab* plane. Here, however, we are able to identify the specific atomic correlations associated with the magnetic ordering.

In Fig. 5(a) we show the temperature dependence of the average in-plane Mn-Mn distance ($\langle$Mn-Mn$\rangle$) and average Ho-Ho distance ($\langle$Ho-Ho$\rangle$). The $\langle$Mn-Mn$\rangle$ distance tracks the changes at all three magnetic ordering temperatures and is consistent with what is observed in the in-plane Mn-O4 distance mentioned above. On the other hand, no change is seen in the $\langle$Ho-Ho$\rangle$ distance except at T_{Ho}. In Fig. 5(b), the short and long Ho-Mn bond distances display intriguing behavior. While the long Ho-Mn bond exhibits (at most) a weak dip at T_{SR}, the short Ho-Mn bond exhibits a strong drop. At T_{Ho} both bonds show sharp changes. Recent powder neutron scattering measurement (RE=Ho, Sc, and Yb) show the importance of the *x* position of the Mn ions (in the unit cell) in determining T_{SR}.[21] In this work we give a detailed picture indicating that, for open $4f$-shell systems such as $HoMnO_3$, the RE-Mn interaction plays an important role at T_{SR}. In
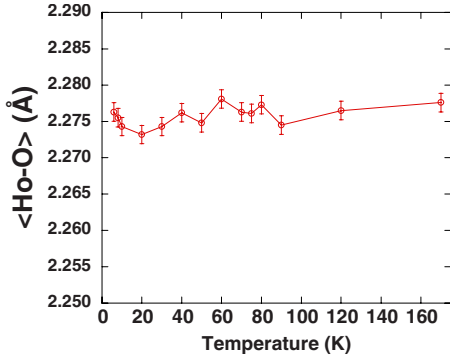
FIG. 6. (Color online) Average Ho-O bond distance as a function of temperature. Note the suggestion of a small "dip" in the region of T_{SR}.

more general terms, in this work, we show the important part played by specific bond pairs involving magnetic ions. For completeness, we now show the average Ho-O distance in Fig. 6. There is a suggestion of a small dip analogous to that of short Mn-Ho bond [Fig. 5(b)] near T_{SR} (between 10 and 40 K) approaching the limit of detectability.

The measurements enable us to assess atomic origin of the magnetic ordering [Fig. 4(b)]. The transition at T_N is driven by strong in-plane Mn-Mn interactions ($J1$) supported by a reduction in the Mn-O4 and Mn-Mn distances. The transition at T_{SR} is related both with the Mn-Mn in-plane correlations ($J1$) and the short Ho-Mn interactions ($J3S$). The transition at T_{Ho}, involves all interactions Mn-Mn ($J1$), Ho-Mn short ($J3S$), Ho-Mn long ($J3L$) and the Ho-Ho interaction ($J2$). We can thus estimate the relative sizes of the exchange interactions $|J1| > |J3S| > |J3L| > |J2|$. Figure 7 shows all interactions discussed.

Recent measurements of the Ho magnetic ordering at low temperature on $HoMnO_3$ single crystals[22] reveal that both the Ho1 and Ho2 sites order with spins along the c-axis and have antiferromagnetic coupling along c ($J5$). With this in mind, the structural changes involving the Ho ions can be under-
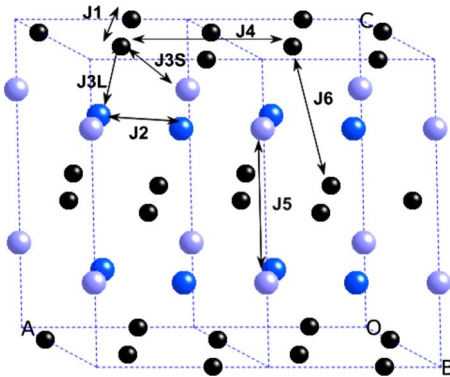

FIG. 7. (Color online) Exchange paths, Ji, for $HoMnO_3$ can be grouped into in-plane Mn-Mn ($J1$) and Ho-Ho ($J2$), Mn-Ho interactions ($J3S$ and $J3L$), and the more distant in-plane Mn-Mn ($J4$) and between plane Mn-Mn ($J5$) and Ho-Ho ($J6$). The close proximity of T_N and T_{SR} indicate that $J1$ and $J3S/J3L$ are similar in magnitude. O, A, B, and C indicate the origin, a, b, and c directions, respectively. Oxygen atoms were excluded for clarity.

stood in terms of a simple model of single-ion magnetic anisotropy.[23] Above the Ho^{3+} ordering temperatures (T_{Ho} and T_{SR}), the spins on the Ho sites are randomly arranged. Because of the high localization of the $4f$ electrons, the crystal field imposed by the oxygen neighbors does not modify the charge distribution of Ho atoms. An atomic picture can thus be used. The Ho^{3+} ion has a highly anisotropic charge distribution with a prolate or pancakelike squashed sphere. The magnetic moment on the Ho^{3+} ions is rigidly coupled to the $4f$ charge density and is parallel to the symmetry axis. Because of the asymmetric shape of these ions rotation of the Ho^{3+} moments must be accommodated by a change in the lattice. This explains the anomalies seen at T_{SR} and T_{Ho} in the local bond distances and in the dielectric constant (first order transitions). Moreover, the phonon modes will be altered as has been observed.

Returning to the origin of the spin rotation at T_{SR}, we note that the directions of spins in magnetically ordered states of transition metal oxides are usually determined by the spin-orbit interaction, or the magnetic anisotropy. The Mn and surrounding three O ions in the plane has the symmetry of isosceles triangles. The two apical Mn-O bond distances are not equal. Such low-local symmetry splits all the Mn $3d$ orbitals, xy, yz, zx, x^2-y^2, and $3z^2-r^2$. With a strong Hunds coupling, Mn is expected to be in a high-spin state, and the four $3d$ electrons occupy xy, yz, zx, and x^2-y^2 orbitals since the average apical Mn-O bond distance is shorter than the average in-plane Mn-O bond distance. Therefore, the empty orbital state above and below T_{SR} should remain identical, $3z^2-r^2$, and the spin-orbit interaction is not likely to change the spin orientation at T_{SR}. It is known that anisotropic exchange interaction, such as $H_{aniso,ex} = \Sigma \vec{S}_i \hat{A}_{i,j} \vec{S}_j$, where $\hat{A}_{i,j}$ is a 3×3 interaction matrix, plays an important role in multiferroic materials. For example, it is suggested that symmetric superexchange interaction and asymmetric Dzyaloshinskii-Moriya interaction contribute anisotropic exchange interaction between Ho and Mn ions in $HoMnO_3$.[1] Unlike usual isotropic Heisenberg exchange interaction, anisotropic exchange interaction depends on the absolute spin orientations in addition to the relative spin orientation. The changes in local structure we have observed near T_{SR} can influence the matrix elements in $\hat{A}_{i,j}$ through magnetostriction effect, which can change the ground-state spin orientation, giving rise to a spin rotation transition at T_{SR}. We also note that the changes in local structures are much more complex than the changes in average structures. It underscores the importance of the local probes for the study of multiferroic materials.

Using a simplified model, the change in bond distances at the magnetic ordering temperatures can be understood in terms of competing spin and lattice energies (see, for example, Ref. 24). The exchange energy $J(x,y,z,\theta) \mathbf{S_i} \cdot \mathbf{S_j}$ for a spin pair is a function of bond distance and bond angle. Atomic displacements result in changes in lattice energy $\delta E_L \sim 1/2 \; k \; (\delta x^2 + \delta y^2 + \delta z^2)$ for a bond pair while the spin contribution for a given pair changes as $dE_J \sim [J(x+\delta x, y+\delta y, z+\delta z, \theta+\delta\theta) - J(x,y,z,\theta)] \; \mathbf{S_i} \cdot \mathbf{S_j}$. The distorted structure at a given temperature will minimize the sum of spin (E_J) and lattice (E_L) contribution to the total energy. Strongly fluctuating local distortions will produce a random spin state

TABLE I. Self-force constants of ions (eV/Å^2).

Ion site	k_x	k_y	k_z
Mn	8	8	27
O1	8	8	16
O2,O3	7	7	9
O4	7	7	7
Ho1	13	13	13
Ho2	13	13	8

while periodic local order will lead to ordered spin states. In this way, local coherent distortions which support a finite polarization are intimately coupled with the magnetic ordering. In the other direction, the magnetic order will be sensitive to the details of the local structures. External perturbations such as pressure, strain and electrical fields, for example, will affect the magnetic ground state. Indeed a rather complex magnetic ground state is found[3,5] and both pressure and substrate strain modify the magnetic properties.[8,11,12]

Analysis of the *x*, *y*, and *z* components of the force constants (self-force constants[25]) on all atoms reveals additional anomalies, which can add to our qualitative description of the structural changes. The self-force constants, which indicate the force on the isolated atom with respect unit displacements, are all positive indicating that the optimized structure is stable with respect to the displacement of individual atoms. The constants (Table I) can be used to estimate changes in energy for atomic displacements. *a-b* plane displacements by 0.005 Å for Mn, O, and Ho ions yield energy changes of approximately 0.1, 0.1, and 0.2 meV (1, 1 and 2 cm^{-1}). These numbers are consistent with shifts observed in Raman, infrared and optical spectra.[9] (Note the large spatial asymmetry in the force constants for Mn and O1 showing the sample is stiffer along the *c* axis. This is supported by recent high pressure infrared and high pressure x-ray diffraction measurements conducted by our group.[10])

To understand the bonding and spin coupling and origin of the electric polarization, we plot the total charge density for constant *y* planes at *y*=0.33 and *y*=0.0. In Fig. 8(a) we can see the Mn-O1-Ho2 (short Mn-Ho) and Mn-O2-Ho2 (long Mn-Ho) distances and similar interactions in Fig. 8(b). The interesting observation to be made about the total charge density of the room temperature structure is the significant *c*-axis asymmetry of the charge density of the O3 and O4 ions as well as the Ho ions. This shows the origin of the electric polarization. (We have found the same distortions of O and Ho in the charge density plots of the high temperature paraelectric phase but with presence of inversion symmetry yields no net polarization.) The asymmetry in the charge density enhances the overlap between Ho ions in neighboring *a-b* planes (~6 Å, *J*5) and explains the antiferromagnetic order of Ho ions observed along the *c* axis.[21] Thus, the electric polarization is expected to couple with the Ho ion magnetization at low temperatures.

IV. SUMMARY

Local structural measurements have been performed on hexagonal multiferroic REMnO$_3$ (RE=Ho) in order to deter-

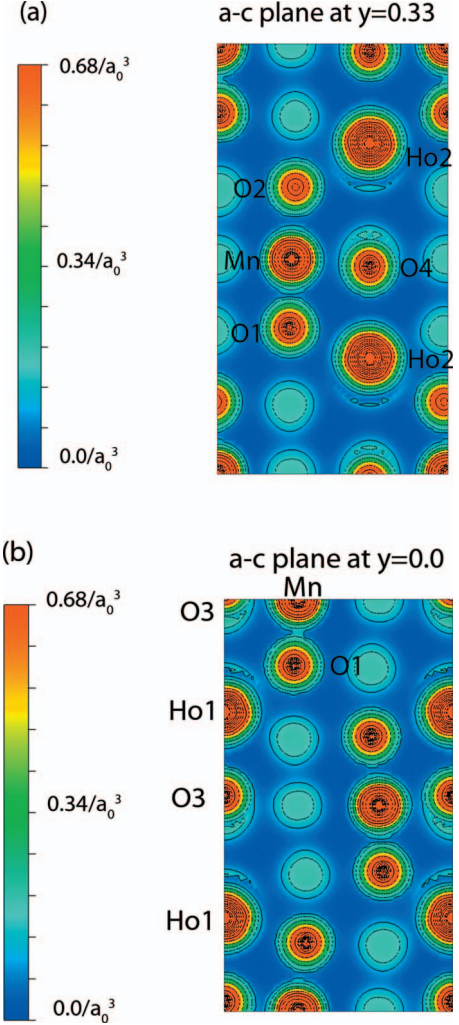FIG. 8. (Color) Charge density plots in atomic units obtained from a DFT calculation for the *a-c* plane at *y*=0.33 [in panel (a)] and *y*=0.0 [in panel (b)]. The origin is in the upper right hand corner and the *z* direction is down. Note the asymmetry in the charge density along the *z* axis for the O3, O4, and Ho atoms which produces the low-temperature polarized state. The Mn-O2-Ho2 in (a) and Mn-O1-Ho1 in (b) are the shortest distance paths, which enable the Mn-Ho coupling.

mine the atomic pairs which are involve in the magnetic ordering transitions and to characterize the spin lattice coupling. The transition from paramagnetic to the antiferromagnetic (noncollinear) phase near ~70 K is dominated by changes in the *a-b* plane Mn-Mn bond distances. The spin rotation transition near ~40 K involves both Mn-Mn and nearest-neighbor Ho-Mn interactions while the low temperature transition below 10 K involves all interactions, Mn-Mn, Ho-Mn (nearest and next nearest) and Ho-Ho correlations. The results show that for RE corresponding to open 4*f*-shell systems, such as HoMnO$_3$, the RE-Mn interaction plays an important role at the Mn spin reorientation temperature T_{SR} and also produce a spin-coupled transition when the RE sites order at low temperatures (below ~10 K). First-principles calculations reveal asymmetric polarization of the charge density of RE=Ho, O3 and O4 sites along the *c* axis in the ferroelectric phase, which facilitates coupling between Ho

atoms on neighboring planes normal to the *c* axis.

[1] T. Lottermoser, T. Lonkai, U. Amann, D. Hohlwein, J. Ihringer, and M. Fiebig, Nature (London) **430**, 541 (2004); M. Fiebig, C. Degenhardt, and R. V. Pisarev, Phys. Rev. Lett. **88**, 027203 (2001).

[2] B. B. Van Aken, T. T. M. Palstra, A. Filippetti, and N. A. Spaldin, Nature Mater. **3**, 164 (2004).

[3] O. P. Vajk, M. Kenzelmann, J. W. Lynn, S. B. Kim, and S.-W. Cheong, Phys. Rev. Lett. **94**, 087601 (2005).

[4] J.-S. Zhou, J. B. Goodenough, J. M. Gallardo-Amores, E. Morán, M. A. Alario-Franco, and R. Caudillo, Phys. Rev. B **74**, 014422 (2006).

[5] B. Lorenz, F. Yen, M. M. Gospodinov, and C. W. Chu, Phys. Rev. B **71**, 014438 (2005).

[6] P. A. Sharma, J. S. Ahn, N. Hur, S. Park, S. B. Kim, S. Lee, J.-G. Park, S. Guha, and S.-W. Cheong, Phys. Rev. Lett. **93**, 177202 (2004).

[7] A. Munoz, J. A. Alonso, M. J. Martinez-Lope, M. T. Casias, J. L. Martinez, and M. T. Fernandez-Diaz, Chem. Mater. **13**, 1497 (2001).

[8] C. dela Cruz, F. Yen, B. Lorenz, Y. Q. Wang, Y. Y. Sun, M. M. Gospodinov, and C. W. Chu, Phys. Rev. B **71**, 060407(R) (2005); T. Katsufuji, S. Mori, M. Masaki, Y. Moritomo, N. Yamamoto, and H. Takagi, *ibid.* **64**, 104419 (2001).

[9] H. Fukumura, S. Matsui, H. Harima, K. Kisoda, T. Takahashi, T. Yoshimura, and N. Fujimura, J. Phys.: Condens. Matter **19**, 365239 (2007); A. P. Litvinchuk, M. N. Iliev, V. N. Popov, and M. N. Gospodinov, *ibid.* **16**, 809 (2004); A. B. Souchkov, J. R. Simpson, M. Quijada, H. Ishibashi, N. Hur, J. S. Ahn, S. W. Cheong, A. J. Millis, and H. D. Drew, Phys. Rev. Lett. **91**, 027203 (2003).

[10] P. Gao, Z. Chen, T. A. Tyson, Z. Liu, J. Hu, C. Zhang, S.-B. Kim, and S.-W. Cheong (unpublished).

[11] P. Murugavel, J.-H. Lee, D. Lee, D. Lee, T. W. Noh, Y. Jo, M.-H. Jing, Y. S. Oh, and K. H. Kim, Appl. Phys. Lett. **90**, 142902 (2007).

[12] I. Gelard, C. Dubourdieu, S. Pailhes, S. Petit, and Ch. Simon, Appl. Phys. Lett. **92**, 232506 (2008).

[13] T. Katsufuji, M. Masaki, A. Machida, M. Moritomo, K. Kato, E. Nishibori, M. Takata, M. Sakata, K. Ohoyama, K. Kitazawa, and H. Takagi, Phys. Rev. B **66**, 134434 (2002); Y. Aikawa, T. Katsufuji, T. Arima, and K. Kato, *ibid.* **71**, 184418 (2005).

[14] C. J. Fennie and K. M. Rabe, Phys. Rev. B **72**, 100103(R) (2005).

[15] B. Ravel and M. Newville, J. Synchrotron Radiat. **12**, 537 (2005); *X-Ray Absorption: Principles, Applications, Techniques of EXAFS, SEXAFS and XANES*, edited by D. C. Konningsberger and R. Prins (Wiley, New York, 1988).

[16] K. V. Klementev, J. Phys. D **34**, 209 (2001).

[17] T. A. Tyson, M. Deleon, S. Yoong, and S. W. Cheong, Phys. Rev. B **75**, 174413 (2007).

[18] A. L. Ankudinov and J. J. Rehr, Phys. Rev. B **56**, R1712 (1997).

[19] G. Kresse and D. Joubert, Phys. Rev. B **59**, 1758 (1999).

[20] K. Schwarz, P. Blaha, and G. K. H. Madsen, Comput. Phys. Commun. **147**, 71 (2002).

[21] X. Fabreges, S. Petit, I. Mirebeau, S. Pailhes, L. Pinsard, A. Forget, M. T. Fernandez-Diaz, and F. Porcher, Phys. Rev. Lett. **103**, 067204 (2009).

[22] P. J. Brown and T. Chatterji, J. Phys.: Condens. Matter **18**, 10085 (2006).

[23] R. Skomski, *Simple Models of Magnetism* (Oxford Press, New York, 2008).

[24] T. E. Saunders and J. T. Chalker, Phys. Rev. B **77**, 214438 (2008).

[25] Ph. Ghosez, E. Cockayne, U. V. Waghmare, and K. M. Rabe, Phys. Rev. B **60**, 836 (1999).